Aalborg Universitet

AALBORG UNIVERSITY
DENMARK

Low Altitude Air-to-Ground Channel Characterization in LTE Network

Cai, Xuesong; Wang, Nanxin; Rodríguez-Piñeiro, José ; Yin, Xuefeng; Pérez Yuste, Antonio ; Fan, Wei; Zhang, Guojin; Pedersen, Gert Frølund; Tian, Li

Low Altitude Air-to-Ground Channel Characterization in LTE Network

Xuesong Cai[1], Nanxin Wang[2], José Rodríguez-Piñeiro[2], Xuefeng Yin[2], Antonio Pérez Yuste[3], Wei Fan[1], Guojin Zhang[1], Gert Frølund Pedersen[1], and Li Tian[4]

[1] Department of Electronic Systems, Aalborg University, Aalborg, Denmark
[2] College of Electronics and Information Engineering, Tongji University, Shanghai, China
[3] School of Telecommunications Engineering, Technical University of Madrid, Madrid, Spain
[4] ZTE Corporation, Shanghai, China
Email: [1]{xuc, wfa, guojin, gfp}@es.aau.dk, [2]{1631501, j.rpineiro, yinxuefeng}@tongji.edu.cn,
[3]antonio.perez@upm.es, [4]tian.li150@zte.com.cn.

Abstract—Low altitude unmanned aerial vehicle (UAV)-aided applications are promising in the future generation communication systems. In this paper, a recently conducted measurement campaign for characterizing the low-altitude air-to-ground (A2G) channel in a typical Long Term Evolution (LTE) network is introduced. Five horizontal flights at the heights of 15, 30, 50, 75, and 100 m are applied, respectively. The realtime LTE downlink signal is recorded by using the Universal Software Radio Peripheral (USRP)-based channel sounder onboard the UAV. Channel impulse responses (CIRs) are extracted from the cell specific signals in the recorded downlink data. To shed lights on the physical propagation mechanisms, propagation graph simulation is exploited. Moreover, path loss at different heights are investigated and compared based on the empirical data. The simulated and empirical results provide valuable understanding of the low altitude A2G channels.

Index Terms—Air-to-ground channel, channel measurements, LTE, graph modeling and path loss

I. Introduction

Recently, the increasing development of unmanned aerial vehicles (UAVs) makes it possible to involve new types of communication applications in the future fifth generation communication systems. The decreasing cost and size of UAVs are promising more widely-applied civil and commercial applications such as video surveillance, search and rescue, precision farming, wildlife monitoring, and transportation, among others [1], [2].Accurate knowledge of the air-to-ground (A2G) channel is essential to enable the low-latency and high-data-rate UAV-based applications.

Considerable efforts have been taken to investigate the A2G channels. Simulation tools [3]–[6] such as ray-tracing and geometry-based stochastic modeling approach were exploited to study the A2G channel characteristics, e.g., the path loss. Regarding the measurement-based investigations, the richest

set can be found in [7], [8]. The considered frequency bands are 968 MHz and 5.06 GHz. The scenarios of interest include suburban, near urban, mountain, desert, hilly, over-sea, etc. Path loss, channel dispersions, fast fading etc. were investigated thoroughly. The UAV applied in these investigations is an aircraft with large size, and its height can be up to 2000 meters. The curved earth two-ray model was generally applied by the authors, due to the fact that at very high altitude only line-of-sight (LoS) and ground-reflected paths have important contributions.

However, many countries have issued regulations limiting the UAVs with maximum heights up to 150 m [9], [10]. Under these constraints, UAV operating in current Long Term Evolution (LTE) networks is promising in the next decade, since it is not likely to built new infrastructures to support low-altitude UAV applications in the near future. Efforts to enable the low altitude UAV applications will be mostly carried out on the UAV side. It is naturally of importance and necessity to investigate the low altitude A2G channels in LTE networks with small UAVs applied. Several measurement based investigations can be found in [9], [11]–[13]. In these works, fading characteristics such as path loss, shadowing and fast fading were investigated. The frequency bands of interest include 800 MHz, 3.1 GHz and 3.5 GHz. Effects of tree foliage [12] and UAV orientations [13] were also addressed.

To enrich the understanding of low altitude A2G channels in the typical LTE networks, a measurement campaign campaign in a LTE network in normal operation has been conducted. Channel impulse responses (CIRs) are estimated from the downlink data received in five horizontal flights at different heights. Propagation graph simulation is exploited to shed lights on the main propagation mechanisms. Further, height dependent path loss is also investigated. The rest of this paper is organized as follows. Sect. II describes the measurement equipments, scenario, and raw data processing. Sect. III elaborates the propagation graph simulation for understanding the propagation mechanisms. Empirical path loss at different heights are discussed in Sect. IV. Finally, conclusive remarks are given in Sect. V.
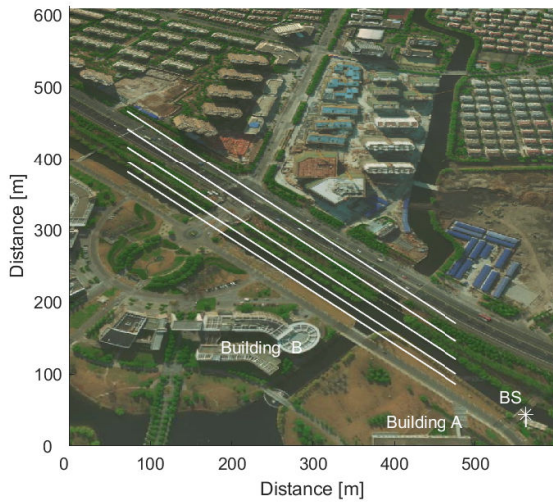
Fig. 1: Satellite view of the measurement scenario and flight routes.

Fig. 2: The six-wings UAV used in the measurement campaign.

Fig. 3: The radiation pattern of the discone antenna measured at 2.585 GHz.

II. MEASUREMENTS AND RAW DATA PROCESSING

Fig. 1 illustrates the scenario where the measurement campaign was conducted. It is a typical suburban scenario with buildings, trees, rivers, etc. at the Jiading Campus of Tongji University, Shanghai, China. The commercial LTE base station (BS) as indicated by the asterisk in Fig. 1 was exploited as the transmitter (Tx). The BS height was about 20 meters, and the center frequency of the LTE downlink signal was 2.585 GHz. Note that the BS is configured for typical downward coverage. However, the specific radiation pattern as well as tilt values are not provided by the network operator. The UAV in operation is illustrated in Fig. 2. The channel sounder onboard the UAV mainly contains the following components: a quasi-omnidirectional discone antenna, a Universal Software Radio Peripheral (USRP) device of type N210 [14], an accurate 10 MHz reference for the USRP, a small computer base unit and a standard WiFi router. The discone antenna works in the frequency band of 1-8 GHz. The 10 MHz reference is disciplined by the Global Positioning System (GPS) signal. The computer base unit is used to control the USRP device and store the received data. The WiFi router was equipped with the only purpose of controlling of the computer remotely during the flights. As indicated by the horizontal lines in Fig. 1, five horizontal round-trip flights at the heights of 15, 30, 50, 75 and 100 m were applied. The realtime downlink signals with bandwidth of 18 MHz were recorded at the center frequency of 2.585 GHz with complex sampling rate of 25 MHz. The location information was also recorded by the built-in function of UAV. Fig. 3 illustrates the radiation pattern of the receiver (Rx) antenna, i.e. the discone antenna, at 2.585 GHz. The Rx antenna is chosen to minimize the effect of its radiation pattern to the channel characteristics in the five horizontal flights. In the offline post-processing, CIRs $h(t,\tau)'s$ are extracted from the measured data mainly according to the steps, i.e., filtering, LTE signal detection and synchronization, and CIR extraction. The detailed steps can be found in [15], [16].
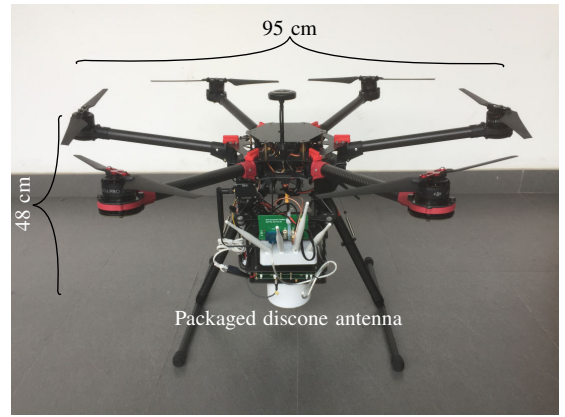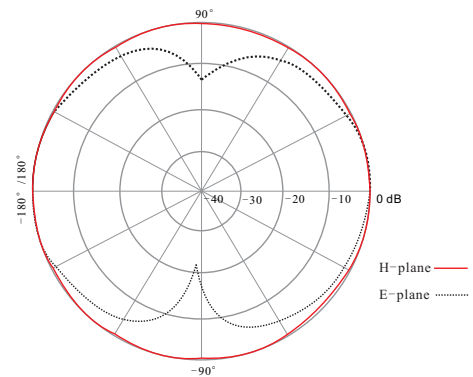
III. PHYSICAL INTERPRETATION

Fig. 4 illustrates an example of concatenated power delay profiles (CPDPs), i.e. $|h(t,\tau)|^2$, for the horizontal flight at the height of 75 meters. It is noteworthy that both the delay and power are relative values because the time synchronization is achieved offline and the transmitted power at BS is unknown. Nevertheless, the link distance can be calculated according to the geometry so that the relative delays can easily be shifted to absolute values. It can be observed from Fig. 4 that the LoS delay trajectory pattern is consistent with the fight route. That is, the propagation distance increased first and then decreased. Besides the LoS trajectory, there are also Non-LoS (NLoS) paths. This indicates the objects that exist in the environment have noneligible contributions to the channel.

To gain insights into how the environment interacts with the transmitted signals, we exploit the propagation graph theory [17], [18] to simulate the CPDPs. The graph simulation tool was firstly proposed in [17] for stochastic channel modeling and is advantage in simulating channels with scattering up to infinite number of interactions in a very efficient way. Later, it was modified in [18] by setting the vertexes and edges according to the environment for semi-deterministic geometrical channel simulation. Readers may refer to [17], [18] for details. Herein, we exploit the graph simulation tool to gain insights into the main propagation mechanisms rather than accurately reproduce the channels. Thus several
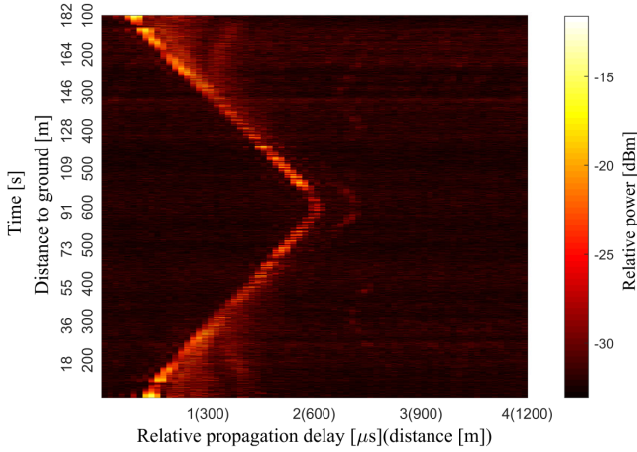
Fig. 4: CPDPs of a horizontal round-trip flight at the height of 75 meters.

Fig. 5: Digital map applied in the propagation graph simulation.

Fig. 6: Simulated CPDPs.

simplifications are applied. The grassland, river, roads etc. are modelled as ground. The buildings materials are set as the same type. The trees and unimportant buildings are not incorporated. The graph simulation is then conducted by four steps which include the 3-dimensional digital map construction, viability evaluation among the vertexes, antenna radiation pattern embedding and channel transfer function (CTF) calculation. Simulated CIRs can be obtained via inverse Fourier Transform from the corresponding CTFs.

Fig. 5 illustrates the 3-D digital map established for the environment which includes the main objects (e.g. buildings A and B) and an example horizontal flight route at 75 m. Fig. 6(a) illustrates the simulated CPDPs[1] for the horizontal flight at 75 m with its corresponding measured CPDPs illustrated in Fig. 4. By comparing the two figures, it can be observed that the main clusters have been reproduced by using the graph simulation tool, which means that the simulation demonstrates clearly the main propagation mechanisms of the channel with rich multipath components. Furthermore, the individual CPDPs contributed by individual objects are illustrated in Figs. 6(b)-(d). Due to the bandwidth limitation, the LoS and ground contribution are nearly non-resolvable. Building A contributes to the signal during the whole flight with larger delay to the LoS component. However, due to the round shape of Building B, its contribution diminishes after the UAV passes away from it.

IV. PATH LOSS

Based on the measured data when all the contributions from the environment are included, path loss at different heights are investigated. The channel power is calculated as

$$p(t) = \sum_{\tau} |\alpha_\ell(t)|^2 \qquad (1)$$

where $|\cdot|$ denotes the absolute value of the argument, and α_ℓ denotes the amplitudes of multipath components estimated

from $h(t, \tau)$ by using the Space-Alternating Generalized Expectation-maximization (SAGE) algorithm. The implementation of SAGE is based on the signal model assumption as

$$h(t, \tau) = \sum_{\ell=1}^{L(t)} \alpha_\ell(t)\delta(\tau - \tau_\ell(t)) + n(t) \qquad (2)$$

where $\delta(\cdot)$, L, n denote the Dirac delta function, path number and noise, repectively. Readers could refer to [19]–[21] for the detailed implementation procedures. Furthermore, fast fading is averaged out by using a sliding window of 20 wavelengths [22].

Fig. 7 illustrates the power variation at different heights. It can be observed that the channel power at 15 m is obviously larger than that observed at the other higher hights. This is reasonable since the LTE BS has a typical downward coverage. When the UAV is above the BS out of its main beam, the received power decreases significantly. A modified close-in free path loss model is exploited herein to model the path loss at different heights as

$$P_\mathrm{L}[\mathrm{dB}] = 10\gamma_h \cdot \log_{10}(d) + X_h + b_h \qquad (3)$$

where γ_h denotes the path loss exponent (PLE), d represents the horizontal distance, X_h is the shadow fading, and b_h

---

[1]Since the measured power is relative, the power of the simulated data is shifted by a certain value for better comparison.
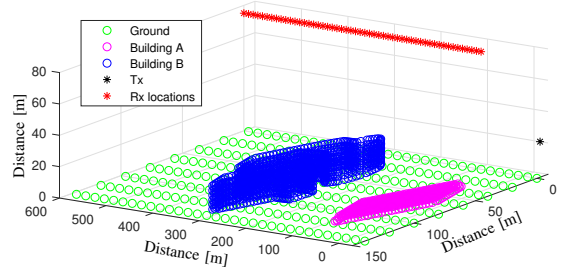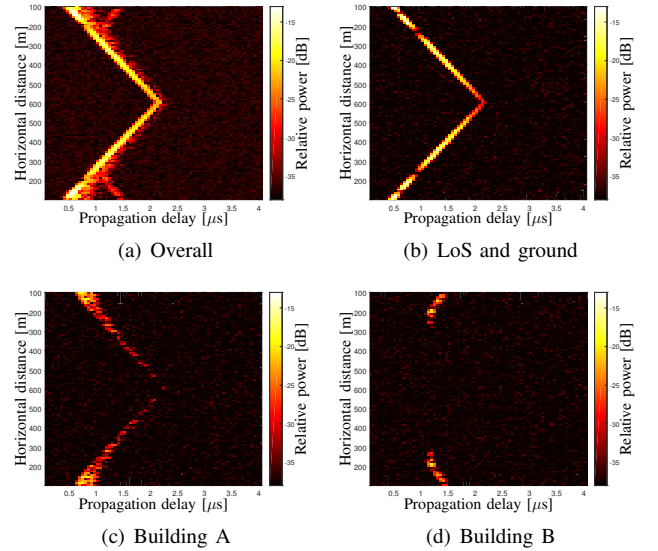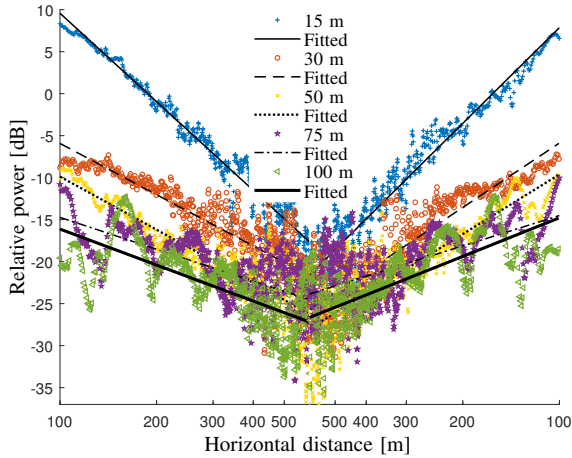
Fig. 7: Power fittings for the five horizontal flights.

Table I: PLEs for the five horizontal flights

Height [m]	15	30	50	75	100
Outbound γ_h	3.50	2.04	2.12	1.34	1.62
Inbound γ_h	3.78	2.56	2.42	1.27	1.73
Mean γ_h	3.64	2.30	2.28	1.31	1.67

indicates the intercept. Note that since the power is relative, b_h is not discussed herein.

The power fittings by using (3) to the five empirical curves are also illustrated in Fig. 7, and the resulted parameters are inclued in Table I. It can be observed that the PLE decreases with the height increasing. We postulate the reasons are as follows. *i)* The LTE BS has downward coverage. The UAV at 15 m is more likely to experience obvious power change by flying out of the main beam. *ii)* When the height of the UAV is larger, the link distance is less sensitive to the horizontal distance. To model the dependence between the heights and the PLEs,

$$\gamma_h = a \cdot h + b + c \tag{4}$$

is used, where a and b are constants, and c is a zero-mean Gaussian-distributed variable. Calculations show that a and b are -0.02 and 3.42, respectively. In addition, the standard deviation of c is 0.48.

V. CONCLUSIONS

In this contribution, a measurement campaign comprising five different horizontal flights was conducted in a LTE network. Propagation graph simulation tool is exploited to investigate the main propagation mechanism of low altitude A2G channels. Unlike the high altitude channels, the low altitude ones consist of rich multipath components contributed by the objects such as buildings that exist on the ground. Moreover, due to the typical downward coverage of LTE BS antenna, the path loss behaviours at different heights are different. Generally, the path loss exponent ranges in 1.6-3.8 with respect to different heights and is negatively correlated with the height. The observations in this contribution provide valuable insights into the low altitude channel. Complete graph

simulation will be applied in the future work to reproduce the channel behaviours, and wideband characteristics will be investigated as well.

REFERENCES

[1] U. D. of Transportation, "Unmanned aircraft system (UAS) service demand 2015-2035: Literature review & projections of future usage," Tech. Rep., Sep 2013, v.0.1 DOT-VNTSC-DoD-13-01.

[2] Y. Zeng, R. Zhang, and T. J. Lim, "Wireless communications with unmanned aerial vehicles: opportunities and challenges," *IEEE Communications Magazine*, vol. 54, no. 5, pp. 36–42, 2016.

[3] E. Tameh, A. Nix, and M. Beach, "A 3-D integrated macro and microcellular propagation model, based on the use of photogrammetric terrain and building data," in *IEEE Vehicular Technology Conference*, vol. 3, 1997, pp. 1957–1961.

[4] W. Khawaja, O. Ozdemir, and I. Guvenc, "UAV air-to-ground channel characterization for mmWave systems," in *IEEE 86th Vehicular Technology Conference (VTC-Fall)*, Sept 2017, pp. 1–5.

[5] N. Schneckenburger, T. Jost, U.-C. Fiebig, G. Del Galdo, H. Jamal, D. Matolak, and R. Sun, "Modeling the air-ground multipath channel," in *IEEE European Conference on Antennas and Propagation (EUCAP)*, 2017, pp. 1434–1438.

[6] M. Wentz and M. Stojanovic, "A MIMO radio channel model for low-altitude air-to-ground communication systems," in *IEEE Vehicular Technology Conference (VTC Fall)*, 2015, pp. 1–6.

[7] D. W. Matolak and R. Sun, "Air-ground channels for UAS: Summary of measurements and models for L- and C-bands," in *2016 Integrated Communications Navigation and Surveillance (ICNS)*, April 2016, pp. 8B2–1–8B2–11.

[8] ——, "Unmanned aircraft systems: Air-ground channel characterization for future applications," *IEEE Vehicular Technology Magazine*, vol. 10, no. 2, pp. 79–85, June 2015.

[9] R. Amorim, H. Nguyen, P. Mogensen, I. Z. Kovács, J. Wigard, and T. B. Sorensen, "Radio channel modeling for UAV communication over cellular networks," *IEEE Wireless Communications Letters*, vol. 6, no. 4, pp. 514–517, Aug 2017.

[10] E. R. S. Group *et al.*, "Roadmap for the integration of civil remotely-piloted aircraft systems into the European aviation system," *European RPAS Steering Group, Tech. Rep*, 2013.

[11] A. Al-Hourani and K. Gomez, "Modeling cellular-to-UAV path-loss for suburban environments," *IEEE Wireless Communications Letters*, vol. 7, no. 1, pp. 82–85, Feb 2018.

[12] W. Khawaja, I. Guvenc, and D. Matolak, "UWB channel sounding and modeling for UAV air-to-ground propagation channels," in *IEEE Global Communications Conference (GLOBECOM)*, 2016, pp. 1–7.

[13] E. Yanmaz, R. Kuschnig, and C. Bettstetter, "Channel measurements over 802.11a-based UAV-to-ground links," in *IEEE GLOBECOM Workshops (GC Wkshps)*, Dec 2011, pp. 1280–1284.

[14] "USRP N210 Datasheet," Tech. Rep. [Online]. Available: https://www.ettus.com/product/details/UN210-KIT

[15] X. Ye, X. Cai, Y. Shen, X. Yin, and X. Cheng, "A geometry-based path loss model for high-speed-train environments in LTE-A networks," in *2016 International Conference on Computing, Networking and Communications (ICNC)*, Feb 2016, pp. 1–6.

[16] X. Cai, J. Pineiro, X. Yin, N. Wang, B. Ai, G. FPedersen, and A. Yuste, "An empirical air-to-ground channel model based on passive measurements in LTE," in *submitted to IEEE Transactions on Vehicular Technology for consideration*.

[17] T. Pedersen and B. H. Fleury, "Radio channel modelling using stochastic propagation graphs," in *IEEE International Conference on Communications*, June 2007, pp. 2733–2738.

[18] L. Tian, V. Degli-Esposti, E. M. Vitucci, and X. Yin, "Semi-deterministic radio channel modeling based on graph theory and ray-tracing," *IEEE Transactions on Antennas and Propagation*, vol. 64, no. 6, pp. 2475–2486, June 2016.

[19] B. Fleury, M. Tschudin, R. Heddergott, D. Dahlhaus, and K. Ingeman Pedersen, "Channel parameter estimation in mobile radio environments using the SAGE algorithm," vol. 17, no. 3, pp. 434–450, 1999.

[20] X. Cai, X. Yin, X. Cheng, and A. P. Yuste, "An empirical random-cluster model for subway channels based on passive measurements in UMTS," *IEEE Transactions on Communications*, vol. 64, no. 8, pp. 3563–3575, Aug 2016.

[21] X. Yin, X. Cai, X. Cheng, J. Chen, and M. Tian, "Empirical geometry-based random-cluster model for high-speed-train channels in UMTS networks," *IEEE Transactions on Intelligent Transportation Systems*, vol. 16, no. 5, pp. 2850–2861, Oct 2015.

[22] W. C. Y. Lee, "Estimate of local average power of a mobile radio signal," *IEEE Transactions on Vehicular Technology*, vol. 34, no. 1, pp. 22–27, Feb 1985.